Quantum Electronics **48** (11) 1035–1042 (2018)

NANOPHOTONICS https://doi.org/10.1070/QEL16777

Effects of near-field electromagnetic coupling in dimers of nanoparticles with a silver core and a J-aggregate dye shell

A.D. Kondorskiy, V.S. Lebedev

Abstract. **We report a theoretical study of the plasmon–exciton coupling effect on the absorption spectra of pairs of closely spaced double-layer hybrid nanoparticles consisting of a metallic core and a J-aggregate dye shell. The effect of frequency conversion of plasmonic lines due to the near-field interaction between plasmons and Frenkel excitons of the organic shell is demonstrated. The effect leads to the appearance of additional spectral lines in the long-wavelength part of the spectrum of the system of hybrid particles. The shapes and the relative intensities of the additional lines exactly reproduce the specific features of the original spectrum of plasmonic absorption bands in uncoated metallic nanoparticles. The discovered phenomenon can be used to design new types of high-sensitivity nanosensors, based on plasmon–exciton effects and principles of near-field optics.**

Keywords: *nanophotonics, dimers of metalorganic nanoparticles, molecular J-aggregates, Frenkel excitons, localised plasmons, plasmon–exciton interaction, near-field electromagnetic coupling, absorption spectra.*

1. Introduction

At present extensive studies of optical properties of various hybrid nanostructures and effects of their interaction with optical fields, including those localised at the nanometre scale, are being carried out. These studies are of great interest for the development of a number of fundamental fields of photonics and plasmonics, subwavelength optics, and physics of quantum-dimensional systems. They are performed in close connection with the development of next generation photonic, optoelectronic and light-emitting devices. In particular, it is worth mentioning the studies in the field of photon and plasmon nanolasers [1–3], optical switches [4, 5], and memory elements [6, 7], nanophotonic integrated circuits [8, 9]. Plasmon, exciton and hybrid nanostructures in the form of nanoantennae are used for field localisation at the nanometre scale similar to the operation of nanowaveguides [10–13] and optical near-field probes [14–19]. Moreover, for certain geometry and structure of composite plasmonic systems, consisting, e.g., of a sequence of metallic nanodiscs of different size, the strength of the local optical fields resulting from their cascade amplification can be extremely high [20].

A.D. Kondorskiy, V.S. Lebedev P.N. Lebedev Physical Institute, Russian Academy of Sciences, Leninsky prosp. 53, 199991 Moscow, Russia; e-mail: kondor@sci.lebedev.ru, vlebedev@sci.lebedev.ru

Received 2 June 2018; revision received 1 August 2018
Kvantovaya Elektronika **48** (11) 1035–1042 (2018)
Translated by V.L. Derbov

A particular role is played by the interdisciplinary research and developments in hybrid organic/inorganic photonics and optoelectronics [21–25] extensively carried out during recent years at the interfaces between new materials science, physics of quantum-dimensional structures, nanoplasmonics, near-field optics, and photochemistry. As an example, one can mention a series of papers on the study of electroluminescence processes in hybrid light-emitting diodes based on quantum dots (QDs) or nanoplatelets (NPLs). These are the so-called QD-OLEDs [26, 27] and NPL-OLEDs [28–30], in which a planar inorganic layer of colloid semiconductor quantum-dimensional structures, located near the interface between the electron and hole transport organic layers of the light-emitting diode, plays the role of its active (emitting) element.

One more significant field in the hybrid organic/inorganic photonics is the study of optical properties of composite nanosystems consisting of metallic nanoparticles and complex molecular J- or H-aggregates of cyanine dyes. The aggregates differ from each other by the packing angle of molecules, which leads to essential difference in their optical properties.

The optical properties of metallic nanoparticles of different shape and size, related to the plasmon resonances arising in them, are well known (see, e.g., [31, 32]). A characteristic feature of dye molecular aggregates is that due to the translation order, the electron excitations in them are collectivised to form Frenkel excitons. J-aggregates of cyanine dyes possess a very narrow optical absorption band, resonance fluorescence with small Stokes shift, anomalously great oscillator strength and high nonlinear optical susceptibility. That is why they attract much interest of researchers related to their possible application for solving numerous fundamental and applied problems of nanophotonics. Recent achievements in the studies of the structure and optical properties of dye molecular aggregates are summarised in review papers [33, 34].

Both the metallic and the molecular subsystem play a key role in the formation of unique optical properties of hybrid metalorganic nanostructures. Their interaction causes so-called plexcitonic (plasmon–exciton) effects [35, 36], arising due to the electromagnetic coupling of Frenkel excitons with localised or travelling surface plasmons, generated in the metallic subsystem under the action of light. Plexcitonic effects in composite planar systems containing dye J-aggregates deposited on a planar metallic substrate were studied in a series of papers by Bellessa et al. (see, e.g., [37, 38]). In the case of interaction between Frenkel excitons and localised surface plasmons, the plexcitonic effects were most actively studied both theoretically and experimentally in two-layer and three-layer metalorganic nanoparticles having different shape and size and consisting of a metallic (Ag, Au)

core and an outer J-aggregate shell (see papers [39–45] and references therein), as well as of metallic nanoshells coated with a layer of a J-aggregate [46]. The main emphasis in recent studies was put on the analysis of optical properties of metal-organic nanostructures in the regime of strong electromagnetic coupling of excitons and plasmons [47–49]. In the regime of strong plexcitonic coupling the hybrid states of the entire system arise that have qualitatively new properties as compared to those of each component considered separately.

Alongside with all mentioned above, in recent years the studies of near-field electromagnetic coupling in systems of a few plasmonic nanoparticles (dimers, trimers, quadrumers) or in their one-dimensional and two-dimensional arrays have become considerably more active (see, e.g., [32, 50–55]). In particular, considerable attention was paid to the study of the properties of plasmonic dimers [56–58]. In addition to that, some experimental works have been recently reported in the literature, devoted to the study of light absorption and scattering spectra in systems of a few plexcitonic nanoparticles or in their arrays [59–64]. However, in contrast to the case of single metalorganic nanoparticles, the physical mechanisms of plasmon–exciton interaction and the general features in the behaviour of near-field electromagnetic coupling in such systems remain practically unknown. Therefore, the theoretical analysis of various plexcitonic phenomena and near-field electromagnetic coupling effects in hybrid nanosystems, consisting of a few metalorganic nanoparticles, is an urgent problem for nanophotonics.

In this paper, we report the computer simulation of spectral properties of pairs of closely spaced (including partial merging) two-layer hybrid nanoparticles, consisting of a silver core coated with a layer of a J-aggregated dye (Fig. 1). The main goal of the study is to determine the optical properties of dimers of metal/J-aggregate nanoparticles and to find new effects in their plexcitonic interaction and near-field electromagnetic coupling of hybrid particles, comprising the dimer. Therefore, for the comparison of results and for deeper understanding of the effect of the outer molecular J-aggregate layer of nanoparticles on the optical properties of the system, we also performed similar calculations in the case of pairs of plasmonic silver nanoparticles without organic coating.

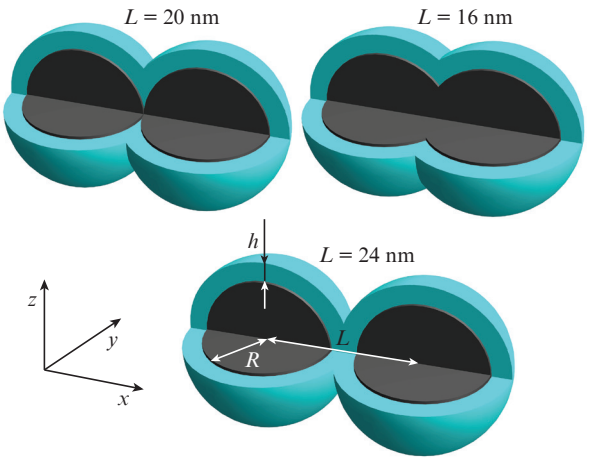

Figure 1. Schematic of the studied plexcitonic systems, consisting of two closely spaced two-layer nanoparticles with a silver core having a radius R and a shell of the J-aggregated cyanine dye having a thickness h. L is the separation between the centres of nanoparticles.

2. Theoretical model

The studied dimers consist of two-layer metalorganic nanoparticles, which represent concentric spheres with a silver core having a radius R = 10 nm, coated with shells of molecular J-aggregates of cyanine dye TC [sodium salt of 3,3′-disulphopropyl-5-5′-dichloro-thiacyanine] having the thickness h = 5 nm. The separation L between the centres of the concentric spheres was varied within a wide range. Figure 1 presents the configurations of the studied nanosystems for L = 16, 20, and 24 nm. For $L < 20$ nm the silver cores of nanoparticles composing the dimer partially merge. In the calculations of spectral properties of a pair of silver nanoparticles without organic coating, their radii were taken to be equal to those of the silver cores of hybrid nanoparticles. Since in this case the 'bare' silver nanoparticles, composing the plasmonic dimer, have no shell, at the distances $L > 20$ nm the particles appear to be completely separated from each other. For both the hybrid plexcitonic dimer and the plasmonic dimer, the surrounding medium was water.

To solve Maxwell's equations in the process of computer modelling of absorption spectra of plexcitonic and plasmonic dimers of nanoparticles studied in the paper we used the finite difference time domain (FDTM) method [65]. Basing on the open source code library MEEP [66] we developed a computer program that allows absorption and scattering cross sections to be calculated for both isolated hybrid nanoparticles and their dimers with the contributions of all multipoles taken into account.

To calculate the absorption and scattering cross sections for a dimer, consisting of a pair of two-layer core–shell nanoparticles, the following theoretical model was used. The computation domain was a parallelepiped, inside which the dimer itself, the field sources and the observation points were located. An absorbing layer surrounded the computation domain with the optical characteristics chosen to provide complete absorption of the light coming from the computation domain (without reflection). To describe the dimer we used the function that determined the dielectric properties of the material as functions of the coordinates. Necessary optical properties were attributed to every point in the computation domain. Depending on the values of the coordinates, it was the permittivity of the metallic core of the studied dimer (Ag), its J-aggregate shell, or the environment (water). At one of the faces of the computation domain the sources were located that generated a plane electromagnetic wave, incident into the computation domain and possessing a given time dependence of the electric field. To study the field scattered by the dimer, it was surrounded by a parallelepiped, at the faces of which in the nodes of a regular mesh, the observation points were located. In the process of computer modelling the values of electric and magnetic field, calculated at these points, were stored in the form of time sequences.

The effective cross sections of absorption (σ_{abs}) and scattering (σ_{scat}) were calculated in the following way: the time dependence of the light from the source was specified in the form of a short pulse having a Gaussian spectrum with the centre frequency in the visible spectral region. For the calculations presented here, the centre wavelength was 500 nm. The pulse duration was usually about three oscillations of the carrier frequency, which was sufficient to obtain results for the entire visible spectral range and near-IR region. The interval of time in which the field dynamics was calculated in the

studied domain was determined by the damping rate of the exciting pulse scattered by the nanostructure, which commonly exceeded the duration of the exciting pulse by many times. In the process of computer modelling, we calculated the time dependences of fields at the points of observation, surrounding the nanoparticle. After completing the simulation, the complex spectral components of electric and magnetic fields $\boldsymbol{E}_\omega(\boldsymbol{r})$ and $\boldsymbol{H}_\omega(\boldsymbol{r})$ were calculated at the observation points using the fast Fourier transform.

Since the calculation of absorption and scattering cross sections implies the determination of perturbation of the process of plane wave propagation introduced by the dimer, for each dimer we performed two calculations, with a dimer and without it. Let us denote by $\boldsymbol{E}_\omega^{(\mathrm{str})}(\boldsymbol{r})$, $\boldsymbol{H}_\omega^{(\mathrm{str})}(\boldsymbol{r})$ and $\boldsymbol{E}_\omega^{(\mathrm{emp})}(\boldsymbol{r})$, $\boldsymbol{H}_\omega^{(\mathrm{emp})}(\boldsymbol{r})$ the respective Fourier components, obtained at the points of observation as a result of computer modelling of scattering and absorption processes. Then the expressions for the cross sections can be written as

$$\sigma_{\mathrm{abs}}(\omega) = \frac{\int \boldsymbol{n}(\boldsymbol{r})\boldsymbol{S}_\omega^{(\mathrm{str})}(\boldsymbol{r})\,\mathrm{d}s}{\left|\boldsymbol{S}_\omega^{(\mathrm{emp})}(\boldsymbol{r}_{\mathrm{cnt}})\right|}, \tag{1}$$

$$\sigma_{\mathrm{scat}}(\omega) = \frac{\int \boldsymbol{n}(\boldsymbol{r})\boldsymbol{S}_\omega^{(\mathrm{diff})}(\boldsymbol{r})\,\mathrm{d}s}{\left|\boldsymbol{S}_\omega^{(\mathrm{emp})}(\boldsymbol{r}_{\mathrm{cnt}})\right|}. \tag{2}$$

The integration is performed over the surface surrounding the dimer (the faces of the parallelepiped with the points of observation). Here, $\boldsymbol{n}(\boldsymbol{r})$ is the normal vector to this surface directed outwards; $\boldsymbol{S}_\omega^{(\mathrm{str})}(\boldsymbol{r})$ is the Poynting vector for the fields obtained as a result of computer simulation of light scattering and absorption by the dimer; $\boldsymbol{S}_\omega^{(\mathrm{diff})}(\boldsymbol{r})$ is the Poynting vector calculated in the absence of a dimer in the centre of the computation domain r_{cnt}:

$$\boldsymbol{S}_\omega^{(\mathrm{str})}(\boldsymbol{r}) = \frac{c}{8\pi}\left[\boldsymbol{E}_\omega^{(\mathrm{str})}(\boldsymbol{r}) \times \left(\boldsymbol{H}_\omega^{(\mathrm{str})}(\boldsymbol{r})\right)^*\right]; \tag{3}$$

$$\boldsymbol{S}_\omega^{(\mathrm{diff})}(\boldsymbol{r}) = \frac{c}{8\pi}\left[\left(\boldsymbol{E}_\omega^{(\mathrm{str})}(\boldsymbol{r}) - \boldsymbol{E}_\omega^{(\mathrm{emp})}(\boldsymbol{r})\right) \times \left(\boldsymbol{H}_\omega^{(\mathrm{str})}(\boldsymbol{r}) - \boldsymbol{H}_\omega^{(\mathrm{emp})}(\boldsymbol{r})\right)^*\right]; \tag{4}$$

$$\boldsymbol{S}_\omega^{(\mathrm{emp})}(\boldsymbol{r}_{\mathrm{cnt}}) = \frac{c}{8\pi}\left[\boldsymbol{E}_\omega^{(\mathrm{emp})}(\boldsymbol{r}_{\mathrm{cnt}}) \times \left(\boldsymbol{H}_\omega^{(\mathrm{emp})}(\boldsymbol{r})\right)^*\right]; \tag{5}$$

and c is the velocity of light in vacuum.

To observe the effects that are the object of this study, it is most convenient to place the pair of particles at the surface, the light being incident normally to it; we modelled the case of equally probable dimer orientations in this plane. The calculation of cross sections was carried out separately for each of two directions of the incident light polarisation, namely, for the polarisation of light along the rotation axis of the system (x axis) and the polarisation of light perpendicular to this axis (y axis) using the formula

$$\langle\sigma\rangle = \frac{1}{2}(\sigma_x + \sigma_y). \tag{6}$$

The absorption and scattering cross sections found in this way correspond to the case of naturally polarised light normally incident on the plane, where the dimers of plexcitonic (Ag/J-aggregate) or plasmonic (Ag) nanoparticles under study are placed.

The optical properties of materials composing the studied dimers of metalorganic nanoparticles are determined by their dielectric functions. The local frequency-dependent dielectric functions of a noble metal can be presented as a sum of contributions of free and bound electrons $\varepsilon(\omega) = \varepsilon_{\mathrm{intra}}(\omega) + \varepsilon_{\mathrm{inter}}(\omega)$. The contribution of free electrons can be described by the Drude formula

$$\varepsilon_{\mathrm{intra}}(\omega) = \varepsilon_\infty^{\mathrm{m}} - \frac{\omega_{\mathrm{p}}^2}{\omega^2 + \mathrm{i}\omega\gamma_{\mathrm{intra}}}. \tag{7}$$

Here, $\omega_{\mathrm{p}} = (4\pi n_{\mathrm{e}} e^2/m_{\mathrm{e}})^{1/2}$ is the plasma frequency; γ_{intra} is the damping coefficient ($1/\gamma_{\mathrm{intra}}$ being the corresponding relaxation time); and $\varepsilon_\infty^{\mathrm{m}}$ is the high-frequency part of the permittivity, related to the contribution of ion cores of the crystal lattice, whereas the contribution of only free electrons taken into account yields $\varepsilon_\infty^{\mathrm{m}} = 1$.

The size of metallic (Ag) cores of nanoparticles composing the studied dimer is chosen smaller than the mean free path length l_∞ of electrons in a bulk metal. Therefore, as in preceding papers [67–70], devoted to the study of plexcitonic effects in single metalorganic nanoparticles, we will consider the size effect, caused by the scattering of free electrons at the surface of a bare metallic particle or at the metal/J-aggregate interface in the calculations of γ_{intra}. For the effective damping coefficient, one can use the known phenomenological expression [71]

$$\gamma_{\mathrm{intra}}^{(R)} = \gamma_{\mathrm{intra}}^{\mathrm{bulk}} + \xi\frac{v_{\mathrm{F}}}{R}, \tag{8}$$

where ξ is the dimensionless constant of the order of unity, the value of which is determined from the comparison with the experimental data on light absorption by metallic particles; and $\gamma_{\mathrm{intra}}^{\mathrm{bulk}} = v_{\mathrm{F}}/l_\infty$ is the decay rate in the bulk metal, determined by the Fermi velocity v_{F} and the mean free path length of electron l_∞.

The contribution of bound electrons (electron transitions between the valence d-band and the conduction sp-band for noble metals) can be calculated in the random phase approximation [72]. Since the contribution of bound electrons is weakly affected by the size effect, the following expression can be used to describe both contributions to the dielectric function of the metallic core with the size effect taken into account,

$$\varepsilon_{\mathrm{m}}(\omega, R) = \varepsilon_{\mathrm{bulk}}(\omega) + \omega_{\mathrm{p}}^2\left(\frac{1}{\omega^2 + \mathrm{i}\omega\gamma_{\mathrm{intra}}^{\mathrm{bulk}}} - \frac{1}{\omega^2 + \mathrm{i}\omega\gamma_{\mathrm{intra}}^{(R)}}\right), \tag{9}$$

following the approach presented in Ref. [71]. Here, $\varepsilon_{\mathrm{bulk}}$ is the permittivity of the bulk metal, obtained from experimental data for Ag [73, 74]; and $\gamma_{\mathrm{intra}}^{(R)}$ is the rate of electron scattering (8) at the metallic particle surface (or at the interface between the metallic core and the organic shell in the case of a hybrid particle). Below we present the parameters, necessary for the Drude formula to calculate the contribution of free electrons to the permittivity of bulk Ag samples and then for Eqn (9) to calculate the frequency- and size-dependent dielectric function $\varepsilon_{\mathrm{Ag}}(\omega, R)$ of a silver nanoparticle from the available experimental data for $\varepsilon_{\mathrm{bulk}}$. In correspondence with the results presented in Refs [75–77], they have the following values: $n_{\mathrm{e}} = 5.85 \times 10^{22}$ cm^{-3}, $\hbar\omega_{\mathrm{p}} = 8.98$ eV, $v_{\mathrm{F}} = 1.4485 \times 10^8$ cm s^{-1}, and $l_\infty = 53.3$ nm.

To demonstrate the size-dependent behaviour of the dielectric function of the silver spherical nanoparticle with the size smaller than the mean free path length of an electron in a bulk metal, Fig. 2 presents the wavelength dependences of the real and imaginary parts of ε for three values of the particle radius R = 5, 10 and 100 nm. The real part of the dielectric function of silver weakly depends on the particle size in the entire spectral range under study. At the same time, the imaginary part Imε essentially depends on the particle size, particularly in the wavelength region, where the contribution of free electrons to the dielectric function appears to be dominant (i.e., for $\lambda \gtrsim 320$ nm for Ag).

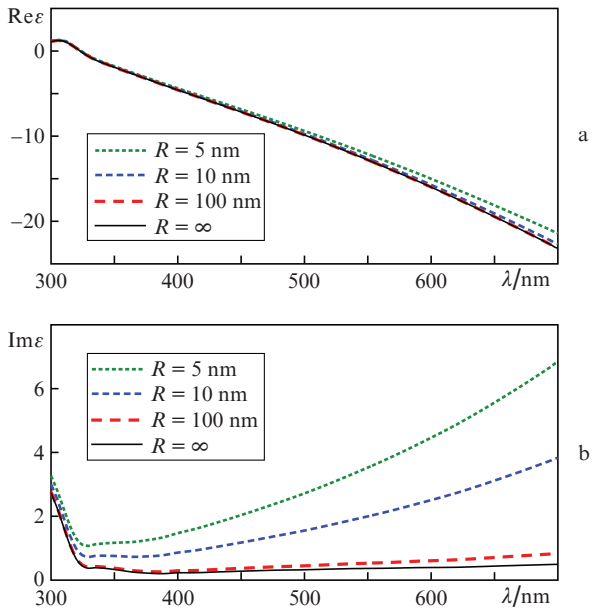

Figure 2. (a) Real and (b) imaginary parts of the dielectric function of silver for different radii of the nanoparticles and for bulk samples (curve $R = \infty$ shows the experimental data [73, 74] for Ag, obtained for the samples with the size considerably exceeding the mean free path length of the electron, l_∞).

In the consideration of plasmon–exciton coupling effects in composite metal/J-aggregate nanosystems, we describe the frequency-dependent dielectric function $\varepsilon_J(\omega)$ of the J-aggregated dye shell using the commonly exploited model of an anharmonic oscillator:

$$\varepsilon_J(\omega) = \varepsilon_J^\infty + \frac{f\omega_0^2}{\omega_0^2 - \omega^2 - i\omega\Gamma}. \qquad (10)$$

Here, the parameters of the Lorentz shape of the dye J-band are determined from the experimental data; ω_0 is the transition frequency, corresponding to the centre of the band; Γ is the full band width; f is the reduced oscillator strength; and ε_J^∞ is the permittivity in the region far from the centre of the absorption J-band. For J-aggregates of the TC cyanine dye studied in the present paper, these parameters, according to Ref. [42], have the following values: $\varepsilon_J^\infty = 1$, $\hbar\omega_0 = 2.61$ eV ($\lambda_0 = 475$ nm), Γ=0.066 eV, and $f = 0.95$. Note that the anharmonic oscillator model satisfactorily describes the spectra of dye J-aggregates, except their asymmetric part.

To obtain more rigorous results in a wide spectral range (including the correct reproduction of asymmetry between the left-hand and right-hand wings of the absorption J-band), the imaginary part of the dielectric function of the J-aggregated cyanine dye can be reconstructed from experimental data on light extinction spectra. Its real part can be also reproduced using the available experimental data by including additional terms of form (10) to the expression for the dielectric function $\varepsilon_J(\omega)$. As already mentioned, all numerical calculations were performed for isolated nanoparticles and their dimers merged in water (environment). Therefore in the calculations for the permittivity of the environment in the visible spectral range we used the value $\varepsilon_w = 1.78$.

Figure 3 presents the calculated dependence of the cross section σ_{abs} of light absorption by isolated metalorganic Ag/J-aggregate nanoparticles on the light wavelength in vacuum λ. The calculations were performed using the general formulae of the modified Mie theory for two concentric spheres [67] with the core radius R = 10 nm and the shell thickness h = 5 nm. In the calculations, we used the parameters of the molecular J-aggregate of the TC cyanine dye that determine the dielectric function (10) of the external organic shell. For the silver core we used the function $\varepsilon_{Ag}(\omega, R)$ [see Eqn (9)]; the obtained cross section of light absorption is shown by the solid curve in Fig. 3. We carried out analogous calculations of the photoabsorption cross section without the size effect taken into account (dashed curve), i.e., using for the metallic core permittivity the function $\varepsilon_{Ag}^{bulk}(\omega)$ of a bulk silver sample. The comparison of the obtained results demonstrates a certain quantitative influence of the size effect on the spectral properties of isolated metalorganic Ag/J-aggregate nanoparticles. It is seen that even in the case of relatively weak plexcitonic electromagnetic coupling of the core and the shell of the hybrid nanoparticle the size effect caused by the scattering of free electrons at the interface between the metallic core and dye J-aggregate shell considerably changes the intensities and widths of spectral peaks of the two-layer nanoparticle. The size effect in the dielectric function of the metallic core of the hybrid metalorganic nanoparticle becomes even more essential under the reduction of the core radius R. This fact is clearly demonstrated by our calculations for R = 5 nm and h = 2.5 nm, the results of which are presented in the inset of Fig. 3. In this context, note that a thorough quantitative analysis of the influence of size effect in the dielectric function of the

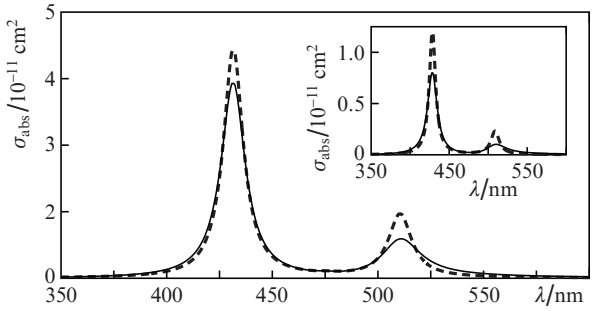

Figure 3. Dependence of the cross section of light absorption by isolated hybrid metalorganic core–shell nanoparticles (Ag/J-aggregated TC cyanine dye) in an aqueous solution on the wavelength of light in vacuum. The solid curve shows the result of calculation, obtained for R = 10 nm and h = 5 nm using Eqns (9) and (10). The dashed curve is obtained using the reference data for the dielectric function of a bulk silver sample. The inset shows the results of analogous calculations for R = 5 nm and h = 2.5 nm.

metallic component (Ag or Au) of isolated hybrid metalorganic nanoparticles on their optical properties was carried out in Refs [40, 67]. Analogous studies for nanoparticles with a metallic shell and a dielectric or semiconductor core were reported in Refs [69, 78, 79].

3. Results and discussion

Figures 4 and 5 present the calculated spectra of light absorption by plexcitonic dimers consisting of two-layer metalorganic Ag/J-aggregate nanoparticles of the TC cyanine dye. Also presented are the results of our calculations for plasmonic dimers, consisting of bare silver nanoparticles. For convenience of the analysis of the spectra of studied systems, Figs 6 and 7 show the spectra of light absorption by these systems, calculated separately for two mutually perpendicular polarisations of the incident radiation, namely, along the axis of the system rotation (the x axis in Fig. 1) and the perpendicular axis (the y axis in Fig. 1). The comparison of the peak positions in the absorption cross sections, obtained for the light polarisation along the axes x and y, with those of the cross sections, averaged over the two possible dimer orientations, allows one to determine the contributions from the 'longitudinal' (σ_x) and 'transverse' (σ_y) electromagnetic modes into the resulting spectra of the studied systems.

As is evident from the figures, the photoabsorption spectrum of a dimer, composed of two similar two-layer metalorganic nanoparticles, consists of two groups of plexcitonic peaks. The bands of the first group are denoted by A, B, C and D. The spectral positions of these peaks weakly change with varying distance between the centres of nanoparticles. The intensity of the dominant absorption band (A) slowly grows with an increase in the distance L. The intensity of the second band of this group (B) slowly falls with increasing L and finally vanishes as the contact between the nanoparticles is broken. The lines C and D are clearly distinguished at L = 28–30 nm, when the organic shells touch each other or slightly overlap. The splitting of line A into lines A, C, and D at the contact of the organic shells is probably analogous to the observed splitting of plasmonic lines 1, 3, and 4 of the bare silver nanoparticles at L = 18–20 nm, which also corresponds to the contact of particles.

The second group of plexcitonic peaks in the absorption spectrum of the systems of two-layer metalorganic nanopar-

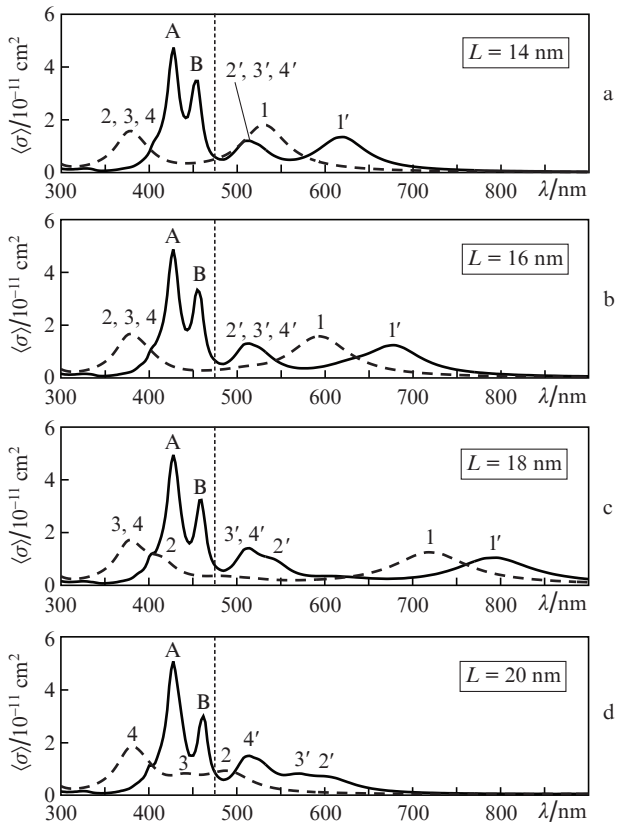

Figure 4. Spectral dependences of cross sections, averaged over two polarisations, for light absorption by plexcitonic dimers, composed by two-layer Ag/TC nanoparticles (solid curves) and plasmonic dimers, composed by two bare silver particles (dashed curves) for different values of L. The vertical dotted line shows the position of the spectral maximum of the absorption band of the J-aggregated TC dye.

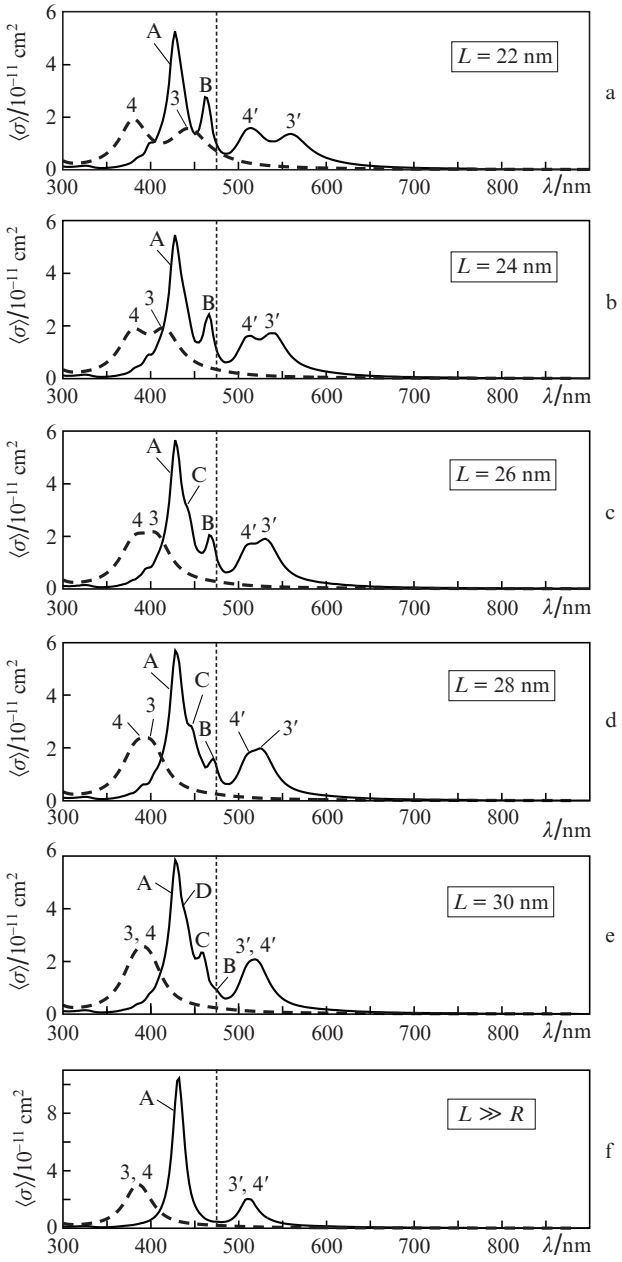

Figure 5. The same as in Fig. 4, but (a–f) for other values of L and (g) the corresponding results of calculation for $L \gg R$.

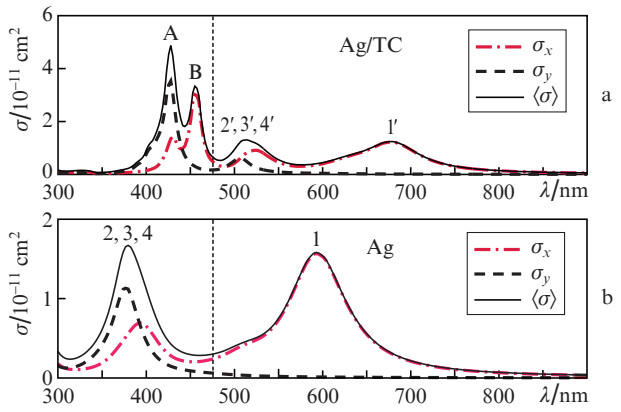

Figure 6. Spectral dependences of (a) light absorption by the systems consisting of the pair of two two-layer Ag/TC nanoparticles and of (b) two bare silver nanoparticles for different polarisations of the incident radiation and $L = 16$ nm. The dash-dotted curves present the absorption cross sections for the polarisation of light along the rotation axis of the system (x axis in Fig. 1). The dashed curves present the absorption cross sections for the light polarisation perpendicular to the rotation axis of the system (y axis in Fig. 1). The solid curves present the absorption cross sections obtained by averaging over two polarisations of light in the xy plane [see Fig. 1 and Eqn (6)]. The vertical dotted line shows the position of the spectral maximum of the J-aggregate absorption band of the TC dye.

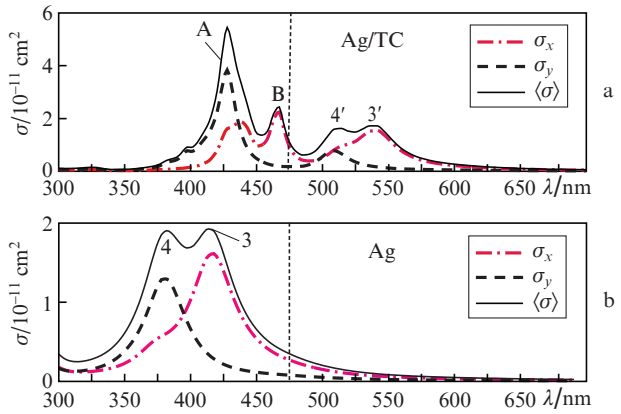

Figure 7. The same as in Fig. 6, but for $L = 24$ nm.

ticles is denoted by 1′, 2′, 3′ and 4′. These lines are located in the long-wavelength part of the spectrum with respect to the lines of the first group, as well as to the position of the spectral maximum of the absorption band of the TC dye J-aggregate ($\lambda = 475$ nm). An important feature of these peaks is that their shapes, mutual positions and relative heights rather exactly repeat the corresponding parameters of the plasmonic peaks in the systems of metallic nanoparticles with the same geometric parameters, but without organic coating (lines 1, 2, 3, and 4). Thus, the near-field electromagnetic coupling of metallic core plasmons with Frenkel excitons of the organic shell leads to the frequency conversion of the plasmonic lines of the cores to the long-wavelength part of the spectrum of two-layer nanoparticles. The detection and study of this effect is the main result of the present paper.

We compare now the variation of parameters of spectral lines 1–4 of the plasmonic dimer, consisting of bare silver nanoparticles, with the variation of parameters of the spectral lines 1′–4′ of the plexcitonic dimer, composed of a pair of similar two-layer nanoparticles Ag/TC, with an increase in the distance L between the centres of nanoparticles. For the distance $L = 14$ nm (see Fig. 4a), two main bands are present in the spectrum of the plasmonic silver dimer, namely, band 1 and a merged group of lines 2, 3 and 4. In the spectrum of the plexcitonic dimer of Ag/TC nanoparticles one can also observe two bands, namely, band 1′ and merged lines 2′, 3′ and 4′ It is important to note that both the relative heights and the mutual arrangement of these bands in the spectrum of the plexcitonic dimer repeat the configuration of bands in the spectrum of a pair of bare silver nanoparticles (without a J-aggregate shell).

This feature is particularly evident when the distance between the core centres of nanoparticles is increased (see Figs 4 and 5). For convenience of interpretation of the obtained spectra, we refer to the plasmonic peaks observed in the system consisting of a pair of silver nanoparticles as 'fundamental peaks', and the plexcitonic peaks repeating their configuration and located in the long-wavelength part of the spectra of dimers consisting of two-layer nanoparticles as 'images'. These notations are conditional and we use them for convenience of identification of specific features in the spectra of the studied dimers of hybrid and metallic nanoparticles.

Peak 1 corresponds to the longitudinal plasmonic mode in a prolate nanostructure, formed by partially merged silver cores (see Fig. 6). When the distance between the centres of the particles increases, this peak shifts to the IR region and vanishes at the breaking of the electric contact between the cores, i.e., at $L > 20$ nm. Image 1′ of peak 1 behaves similarly. At first the position of peak 1′ maximum shifts to the right of the wavelength scale with increasing distance L between the particles of dimer. Then this peak merely vanishes, as the electric contact between the cores of the system becomes broken.

The main plasmonic peak of the silver core, line 4, corresponds to the transverse mode of the silver cores (see Figs 6 and 7); therefore, its spectral position and the value of photoabsorption cross section weakly depend on the distance between the centres of silver cores. Analogous conclusions can be made for its image, peak 4′.

With an increase in the distance L from 14 to 20 nm, the band in the spectrum of a pair of silver nanoparticles, formed by merged lines 2, 3, and 4, splits. This splitting is particularly expressed when the metallic cores touch each other. This is, probably, due to the presence of sharp angles between the surfaces of nanoparticles near the point of their contact. Arising peaks 2 and 3 belong to the longitudinal modes (see Figs 6 and 7). In contrast to the longitudinal plasmonic mode 1 that exists in the presence of electric contact between the silver cores, modes 2 and 3 arise due to near-field coupling of silver cores.

For the distances $L > 20$ nm the electric contact between the silver nanoparticles (and, correspondingly, between the cores of two-layer Ag/TC nanoparticles) is lost and the interaction is implemented via the near-field electromagnetic coupling. Line 2 vanishes, and remaining lines 3 and 4 correspond to the longitudinal and transverse electromagnetic modes of the system. A further increase in the distance L is accompanied by the fall of the interaction efficiency, and peaks 3 and 4 quickly approach each other and merge at $L \gg R$ (see Fig. 5f).

The images of the plasmonic peaks of two bare silver nanoparticles in the spectra of a plexcitonic dimer, formed by a pair of Ag/TC nanoparticles (lines 1′–4′) repeat the finest

details of the splitting evolution of fundamental plasmonic peaks 1–4 . This is particularly obvious in Figs 4c,d and 5a,b, when the spectrum of plasmonic lines of silver nanoparticles appears to be sufficiently complex and contains a large number of separate lines. It is important that the frequency conversion of plasmonic spectral lines of a pair of silver cores into the long-wavelength region occurs both for longitudinal and for transverse electromagnetic modes (see Figs 6 and 7). Thus, we can conclude that in the considered metalorganic nanosystems the plasmonic modes interact with Frenkel excitons practically independently.

The analysis of spectra presented by us also allows the spectra of single metalorganic nanoparticles (see Fig. 5f) to be interpreted in terms of fundamental lines and their images. Indeed, lines 3′ and 4′ are images of lines 3 and 4. In a single spherically symmetric system it is hard to notice this fact, since the modes, corresponding to peaks 3 and 4 are degenerate. A deformation of the metallic core shape or a sufficiently strong near-field electromagnetic coupling with another system can remove this degeneracy, demonstrating the above effect of appearance of plexcitonic images of the fundamental plasmonic lines.

4. Conclusions

We have presented the computer modelling of spectral properties of dimers of closely spaced two-layer hybrid nanoparticles, consisting of a silver core and a shell of the J-aggregated TC dye. The analysis of changes in absorption spectra arising due to variation in the distance between the centres of nanoparticles has shown that the near-field coupling of plasmonic modes of the silver cores with Frenkel excitons of the organic shell leads to the frequency conversion of plasmonic lines into the long-wavelength part of the spectrum. This effect causes the appearance of additional spectral bands, the shape and relative intensities of which rather exactly repeat the spectral features of plasmonic bands of the bare silver cores. We conclude that in the studied hybrid system of metalorganic nanoparticles the plasmonic modes interact with Frenkel excitons almost independently. The detected phenomenon of frequency conversion allows new interpretation of the spectra of single metalorganic nanoparticles, in which the plasmonic modes of metallic cores appear to be degenerate because of spherical symmetry. This effect can be used for designing new types of nanosensors, in which the spectral positions of hybrid plasmon–exciton resonances in nanostructures are sensitive to the changes in the electromagnetic properties of the environment.

Acknowledgements. The work was supported by the Russian Science Foundation (Grant No. 14-22-00273).

References

1. Wang S., Wang X.-Y., Li B., Chen H.-Z., Wang Y.-L., Dai L., Oulton R.F., Ma R.-M. *Nature Commun*., **8**, 1889 (2017).
2. Wang Z., Meng X., Kildishev A.V., Boltasseva A., Shalaev V.M. *Laser Photon. Rev*., **11**, 1700212 (2017).
3. Xavier J., Vincent S., Meder F., Vollmer F. *Nanophotonics*, **7**, 1 (2018).
4. Agrawal A., Susut C., Stafford G., Bertocci U., McMorran B., Lezec H.J., Talin A.A. *Nano Lett*., **11**, 2774 (2011).
5. Xu T., Walter E.C., Agrawal A., Bohn C., Velmurugan J., Zhu W., Lezec H.J., Talin A.A. *Nature Commun*., **7**, 10479 (2016).
6. Rezvanova A.A., Frolova L.A., Troshin P.A. *Mendeleev Commun*., **26**, 26 (2016).
7. Mosciatti T., Bonacchi S., Gobbi M., Ferlauto L., Liscio F., Giorgini L., Orgiu E., Samorì P. *ACS Appl. Mater. Interfaces*, **8**, 6563 (2016).
8. Piracha A.H., Rath P., Ganesan K., Kühn S., Pernice W.H.P., Prawer S. *Nano Lett*., **16**, 3341 (2016).
9. Dai D. *J. Lightwave Technol*., **35**, 572 (2017).
10. Kuznetsova T.I., Lebedev V.S. *Quantum Electron*., **32**, 727 (2002) [*Kvantovaya Elektron*., **32**, 727 (2002)].
11. Kuznetsova T.I., Lebedev V.S. *Phys. Rev. E*, **78**, 016607 (2008).
12. Chen Z.-X., Wu Z.-J., Ming Y., Zhang X.-J., Lu Y.-Q. *AIP Adv*., **4**, 017103 (2014).
13. Fang Y., Sun M. *Light: Sci. Appl*., **4**, 294 (2015).
14. Kuznetsova T.I., Lebedev V.S., Tsvelik A.M. *J. Opt. A: Pure Appl. Opt*., **6**, 338 (2004).
15. Kuznetsova T.I., Lebedev V.S. *JETP Lett*., **79**, 62 (2004) [*Pis'ma Zh. Eksp. Teor. Fiz.*, **79**, 70 (2004)].
16. Kuznetsova T.I., Lebedev V.S. *Phys. Rev. B*, **70**, 035107 (2004).
17. Gramotnev D.K., Bozhevolnyi S.I. *Nature Photon*., **8**, 13 (2014).
18. Kazantsev D.V., Kuznetsov E.V., Timofeev S.V., Shelaev A.V., Kazantseva E.A. *Phys. Usp*., **60**, 259 (2017) [*Usp. Fiz. Nauk*, **187**, 277 (2017)].
19. Bazylewski P., Ezugwu S., Fanchini G. *Appl. Sci*., **7**, 973 (2017).
20. Kravets V.G., Zoriniants G., Burrows C.P., Schedin F., Casiraghi C., Klar P., Geim A.K., Barnes W.L., Grigorenko A.N. *Phys. Rev. Lett*., **105**, 246806 (2010).
21. Agranovich V.M., Gartstein Yu.N., Litinskaya M. *Chem. Rev*., **111**, 5179 (2011).
22. Sanchez C., Belleville P., Popall M., Nicole L. *Chem. Soc. Rev*., **40**, 696 (2011).
23. Aleshin A.N. *Phys. Usp*., **56**, 627 (2013) [*Usp. Fiz. Nauk*, **183**, 657 (2013)].
24. Vitukhnovskii A.G. *Phys. Usp*., **56**, 623 (2013) [*Usp. Fiz. Nauk*, **183**, 653 (2013)].
25. Pushkarev A.P., Bochkarev M.N. *Russ. Chem. Rev*., **85** (12), 1338 (2016) [*Usp. Khim*., **85**, 1338 (2016)].
26. Vashchenko A.A., Lebedev V.S., Vitukhnovskii A.G., Vasiliev R.B., Samatov I.G. *JEPT Lett*., **96**, 113 (2012) [*Pis'ma Zh. Eksp. Teor. Fiz*., **96**, 118 (2012)].
27. Shirasaki Y., Supran G.J., Bawendi M.G., Bulović V. *Nature Photon*., **7**, 13 (2013).
28. Chen Z., Nadal B., Mahler B., Aubin H., Dubertret B. *Adv. Funct. Mater*., **24**, 295 (2014).
29. Vashchenko A.A., Vitukhnovskii A.G., Lebedev V.S., Selyukov A.S., Vasiliev R.B., Sokolikova M.S. *JEPT Lett*., **100**, 86 (2014) [*Pis'ma Zh. Eksp. Teor. Fiz*., **100**, 94 (2014)].
30. Vitukhnovsky A.G., Lebedev V.S., Selyukov A.S., Vashchenko A.A., Vasiliev R.D., Sokolikova M.C. *Chem. Phys. Lett*., **619**, 185 (2015).
31. Lindquist N.C., Nagpal P., McPeak K.M., Norris D.J., Oh S.-H. *Rep. Prog. Phys*., **75**, 036501 (2012).
32. Jiang N., Zhuo X., Wang J. *Chem. Rev*., **118**, 3054 (2018).
33. Bricks J.L., Slominskii Yu.L., Panas I.D., Demchenko A.P. *Methods and Applications in Fluorescence*, **6**, 012001 (2018).
34. Hestand N.J., Spano F.C. *Chem. Rev*., **118**, 7069 (2018).
35. Törmä P., Barnes W.L. *Rep. Prog. Phys*., **78**, 013901 (2015).
36. Cao E., Lin W., Sun M., Liang W., Song Y. *Nanophoton*., **7**, 145 (2018).
37. Bellessa J., Symonds C., Vynck K., Lemaitre A., Brioude A., Beaur L., Plenet J.C., Viste P., Felbacq D., Cambril E., Valvin P. *Phys. Rev. B*, **80**, 033303 (2009).
38. Bellessa J., Symonds C., Laverdant J., Benoit J.-M., Plenet J.C., Vignoli S. *Electronics*, **3**, 303 (2014).
39. Wiederrecht G.P., Wurtz G.A., Bouhelier A. *Chem. Phys. Lett*., **461**, 171 (2008).
40. Lebedev V.S., Vitukhnovsky A.G., Yoshida A., Kometani N., Yonezawa Y. *Colloids and Surfaces A: Physicochem. Eng. Aspects*, **326**, 204 (2008).
41. Lebedev V.S., Medvedev A.S., Vasiliev D.N., Chubich D.A., Vitukhnovskii A.G. *Quantum Electron*., **40**, 246 (2010) [*Kvantovaya Elektron*., **40**, 246 (2010)].
42. Yoshida A., Kometani N. *J. Phys. Chem. C*, **114**, 2867 (2010).
43. Antosiewicz T.J., Apell S.P., Shegai T. *ACS Photon*., **1**, 454 (2014).

44. Laban B., Vodnik V., Vasić V. *Nanospectroscopy*, **1**, 5460 (2015).
45. DeLacy B.G., Miller O.D., Hsu C.W., Zander Z., Lacey S., Yagloski R., Fountain A.W., Valdes E., Anquillare E., Soljačić M., Johnson S.G., Joannopoulos J.D. *Nano Lett*., **15**, 2588 (2015).
46. Fofang N.T., Park T.-H., Neumann O., Mirin N.A., Nordlander P., Halas N.J. *Nano Lett*., **8**, 3481 (2008).
47. Balci S. *Opt. Lett*., **38**, 4498 (2013).
48. Shapiro B.I., Tyshkunova E.S., Kondorskii A.D., Lebedev V.S. *Quantum Electron*., **45**, 1153 (2015) [*Kvantovaya Elektron*., **45**, 1153 (2015)].
49. Todisco F., De Giorgi M., Esposito M., De Marco L., Zizzari A., Bianco M., Dominici L., Ballarini D., Arima V., Gigli G., Sanvitto D. *ACS Photon*., **5**, 143 (2018).
50. Fan J.A., Bao K., Wu C., Bao J., Bardhan R., Halas N.J., Manoharan V.N., Shvets G., Nordlander P., Capasso F. *Nano Lett*., **10**, 4680 (2010).
51. Ye J., Wen F., Sobhani H., Lassiter J.B., Van Dorpe P., Nordlander P., Halas N.J. *Nano Lett*., **12**, 1660 (2012).
52. Lovera A., Gallinet B., Nordlander P., Martin O.J.F. *ACS Nano*, **7**, 4527 (2013).
53. Schlather A.E., Large N., Urban A.S., Nordlander P., Halas N.J. *Nano Lett*., **13**, 3281 (2013).
54. Hu Q., Jin D., Xiao J., Nam S.H., Liu X., Liu Y., Zhang X., Fang N.X. *PNAS*, **114**, 10017 (2017).
55. Bazgir M., Novin S.N., Zarrabi F.B., Heydari S., Arezoomand A.S. *Electromagnetics*, **38**, 207 (2018).
56. Romero I., Aizpurua J., Bryant G.W., Garcia de Abajo F.J. *Opt. Express*, **14**, 9988 (2006).
57. Slablab A., Xuan L.L., Zielinski M., de Wilde Y., Jacques V., Chauvat D., Roch J.F. *Opt. Express*, **20**, 220 (2012).
58. Flauraud V., Bernasconi G.D., Butet J., Alexander D.T.L., Martin O.J.F., Brugger J. *ACS Nano*, **11**, 3485 (2017).
59. Todisco F., D'Agostino S., Esposito M., Fernández-Domínguez A.I., De Giorgi M., Ballarini D., Dominici L., Tarantini I., Cuscuná M., Sala F.D., Gigli G., Sanvitto D. *ACS Nano*, **9**, 9691 (2015).
60. Wang H., Toma A., Wang H.Y., Bozzola A., Miele E., Haddadpour A., Veronis G., De Angelis F., Wang L., Chen Q.D., Xu H.L., Sun H.B., Zaccaria R.P. *Nanoscale*, **8**, 13445 (2016).
61. Ferdele S., Jose B., Foster R., Keyes T.E., Rice J.H. *Opt. Mater*., **72**, 680 (2017).
62. Liu B., Yan H., Stosch R., Wolfram B., Bröring M., Bakin A., Schilling M., Lemmens P. *Nanotechnology*, **28**, 195201 (2017).
63. Song G., Feng X., Duan G.-Y., Chen Y.-Y., Wang C., Zhang P.-F., Yu L. *Plasmonics*, **13**, 1403 (2017).
64. Ralević U., Isić G., Vasić Anicijević D., Laban B., Bogdanović U., Lazović V.M., Vodnik V., Gajić R. *Appl. Surface Sci*., **434**, 540 (2018).
65. Taflove A., Hagness S.C. *Computational Electrodynamics: The Finite-Difference Time-Domain Method* (Norwood: Artech House, 2005).
66. https://meep.readthedocs.io.
67. Lebedev V.S., Medvedev A.S. *Quantum Electron*., **42**, 701 (2012) [*Kvantovaya Elektron*., **42**, 701 (2012)].
68. Lebedev V.S., Medvedev A.S. *J. Russ. Laser Res*., **34** (4), 303 (2013).
69. Lebedev V.S., Medvedev A.S. *Quantum Electron*., **43**, 1065 (2013) [*Kvantovaya Elektron*., **43**, 1065 (2013)].
70. Kondorskiy A.D., Kislov K.S., Lam N.T., Lebedev V.S. *J. Russ. Laser Res*., **36**, 175 (2015)].
71. Kreibig U., Vollmer M. *Optical Properties of Metal Clusters* (Berlin: Springer, 1995).
72. Pines D., Noziéres P. *The Theory of Quantum Liquids* (California: Addison-Wesley, 1989).
73. Johnson P.B., Christy R.W. *Phys. Rev. B*, **6**, 4370 (1972).
74. Babar S., Weaver J.H. *Appl. Opt*., **54**, 477 (2015).
75. *Handbook of Optical Constants of Solids II*. Ed. by E.D.Palik (San Diego: Academic, 1991).
76. Haynes W.M. *Handbook of Chemistry Physics* (Boca Raton: CRC Press, 2014).
77. Gall D. *J. Appl. Phys*., **119**, 085101 (2016).
78. Khlebtsov N.G. *Quantum Electron*., **38**, 504 (2008) [*Kvantovaya Elektron*., **38**, 504 (2008)].
79. Khlebtsov B.N., Liu Z., Ye J., Khlebtsov N.G. *J. Quant. Spectrosc. Radiat. Transfer*, **167**, 64 (2015).